Chalcogenide Letters Vol. 19, No. 12, December 2022, p. 871 - 883

Effect of Ce and Sm doping on optoelectronic and thermoelectric properties of Bi_2Te_3 alloy

M. Jawad[a], S. Selvaraju[b], M. U. Javed [a], F. Ali[a], Q. Rafiq[c],
I. Ur Rahman[a], B. Masood[a], M. B. Hussain[d], S. Azam[a*], H. Elhosiny Ali[e,f]
[a]*Faculty of Engineering and Applied Sciences, Department of Physics, RIPHAH International University, Islamabad, Pakistan.*
[b]*Department of Engineering, University of Technology and Applied Sciences-Salalah, Oman.*
[c]*Department of Physics, Faculty of Basic and applied Sciences, International Islamic University, Islamabad, Pakistan.*
[d]*,Department of Physics, RIPHAH International University, Faisalabad, Pakistan*
[e]*Research center for Advanced Materials Science (RCAMS), King Khalid University, Abha 61413, P.O Box 9004, Saudi Arabia.*
[f]*Physics Department, Faculty of Science, Zagazig University, Zagazig, Egypt.*

Metallic materials attracted much attention in the field of optoelectronics for several applications such as infrared radiation detection. In present study, electronic, optical and thermoelectric spectra of Sm and Ce co doped Bi_2Te_3 materials have been studied using density functional theory (DFT) calculations. Electronic study of the studied material indicates metallic and good optical and thermoelectric properties. Optical spectra of the doped Bi_2Te_3 show that absorption lies in visible and near UV region of the radiation. Thus, it seems to have potential applications in optoelectronics. Thermoelectric properties favor the semiconducting nature with high Seebeck coefficient and dominant character of p-type charge carriers.

(Received February 27, 2022; Accepted December 1, 2022)

Keywords: optoelectronic properties, thermoelectric properties, Doping, Alloy

1. Introduction

The dimensional less figure of merit $ZT = \sigma S^2 T / \kappa$, where σ is the electrical conductivity, S is the Seebeck coefficient, and κ is the thermal conductivity at a particular absolute temperature [1-3], is an evaluation index for the performance of thermoelectric materials. The high performance (ZT) of thermoelectric materials can be attained from reduced thermal conductivity (κ) [4], as expected from the equation. Many thermoelectric materials have been explored to improve thermoelectric performance, including GeTe [5], PbTe [6,7], Bi2Te3 [8, and silicides [9].

Bismuth telluride (Bi2Te3) is a promising thermoelectric material for applications near room temperature. To increase the thermoelectric performance of this material, its dimensions and thermal transport should be decreased. Bi2Te3 is a semiconductor and if it is mixed with antimony or selenium then it can be used as an excellent thermoelectric material for refrigeration. Bismuth telluride is a narrow-gap layered semiconductor with a trigonal unit cell. The valence and conduction band structure can be described as a many-ellipsoidal model with 6 constant-energy ellipsoids that are centered on the reflection planes[10].

Bi2Te3 cleaves easily along the trigonal axis due to Van der Waals bonding between neighboring tellurium atoms. Due to this, bismuth-telluride-based materials used for power

---

[*] Corresponding author: sikandar.azam@riphah.edu.pk
https://doi.org/10.15251/CL.2022.1912.871

generation or cooling applications must be polycrystalline. Furthermore, the Seebeck coefficient of bulk Bi2Te3 becomes compensated around room temperature, forcing the materials used in power-generation devices to be an alloy of bismuth, antimony, tellurium, and selenium[11].

Bi2Te3-based materials are the most sophisticated thermoelectric materials on the market, notably at room temperature [12-20]. Increasing the concentration of point defects in a material is an effective technique to reduce its thermal conductivity, especially for phonons in the high frequency band [4]. From nanostructuring studies, Chen et al. obtained a remarkable ZT value of 1.4 at 473 K [12,13]. It was 1.5 times greater than zone melting values [10,11]. The crystal structure of a Bi2Te3 material is rhombohedral, with a quintuple layer order of –Te(1)-Bi-Te(2)-Bi-Te(1)- [14]. The weak van der Waals link (vdW) between the two quintets tends to cause cleavage in the lamellar-structured single crystal [14]. The crack spreads perpendicular to the surface along their basal planes c–axis resultantly [14].

2. Computational details

By solving Kohn-Sham equations [21] as deployed in the WIEN2k package, the first principle calculations were performed by the full potential linearized augmented plane wave (FP-LAPW) approach under the formulism of density functional theory (DFT) [22-24]. The Bi2Te3 Crystallographic Information Files (CIFs) were collected from the free crystal structure from Materials Project [25] For estimating the various properties, one of the alternative forms of the generalized gradient approximation (GGA) with the exchange correlation potential proposed by Perdew-Burke-Ernzerhof, popularly known as PBE-GGA functional [26] and the hubbard parameter U=7.0 eV were used. The self-consistent cycle (SCF) was performed until a value of 0.0001 Ry and 0.001e were reached by the energy and charge convergence respectively. The same structure file is used for the calculations of the optical and thermoelectric (TE) properties, a denser k-mesh of 10 × 10 × 10 with 1000 k-points in the full Brillouin zone (FBZ) was used.

3. Results and discussion

Alloy can be formed by mixing metal with another metal or a non-metal. For example, red gold can be made if we mix gold with copper, white gold can also be prepared by the mixture of gold and silver and silver combines with copper to produce sterling silver. Similarly, by combining iron with non-metallic carbon or silicon we can get steel or silicon steel. The material produced because of this mixing has different properties than pure metals like strength or hardness increases.

3.1. The density of states

The density of states (DOS) is essentially the number of different states at a particular energy level that electrons can occupy, i.e., the number of electronic states per unit volume per unit energy. Bulk properties such as specific heat, paramagnetic susceptibility, and other transport phenomena of conductive solids depend on this function. DOS calculations allow one to determine the general distribution of states as a function of energy and can also determine the spacing between energy bands in semi-conductors [41]. Semiconducting materials exhibit a typical electronic band structure that is determined by contribution of different electronic states in the valance and conduction bands. The density of states helps us to explore electronic and their atomic and orbital origins. Using GGA+ U and LDA + U approximations, we have calculated the total density of states (TDOS) and partial density of states (PDOS).

Figure 2 (a-f) shows the total and partial density of state profile in the energy range between -6 eV to + 6eV. Figure 2 (e) shows the partial density of states for Ce, Sm, Bi and Te. In the region of valence band, the first valence band located near fermi level is strongly dominated by Sm-d orbital (see fig 2(d)). The second valence band is seen at energy almost equal to -5.0ev which is dominated by Ce-f indicated in figure 2(c). On the other hand, in the region of conduction band, the first band is seen between energy 1.0 eV to 2.0 eV which is strongly dominated by Ce-f orbital with small contribution of Te-p orbital.

From fig 2 (f) as band gap in the valence bands is very small which confirms that our material Bismuth Telluride (Bi_2Te_3) is a semiconductor. In the region of conduction band, we can see that up and down states are not the same they are different which confirms that there are no magnetic moments.

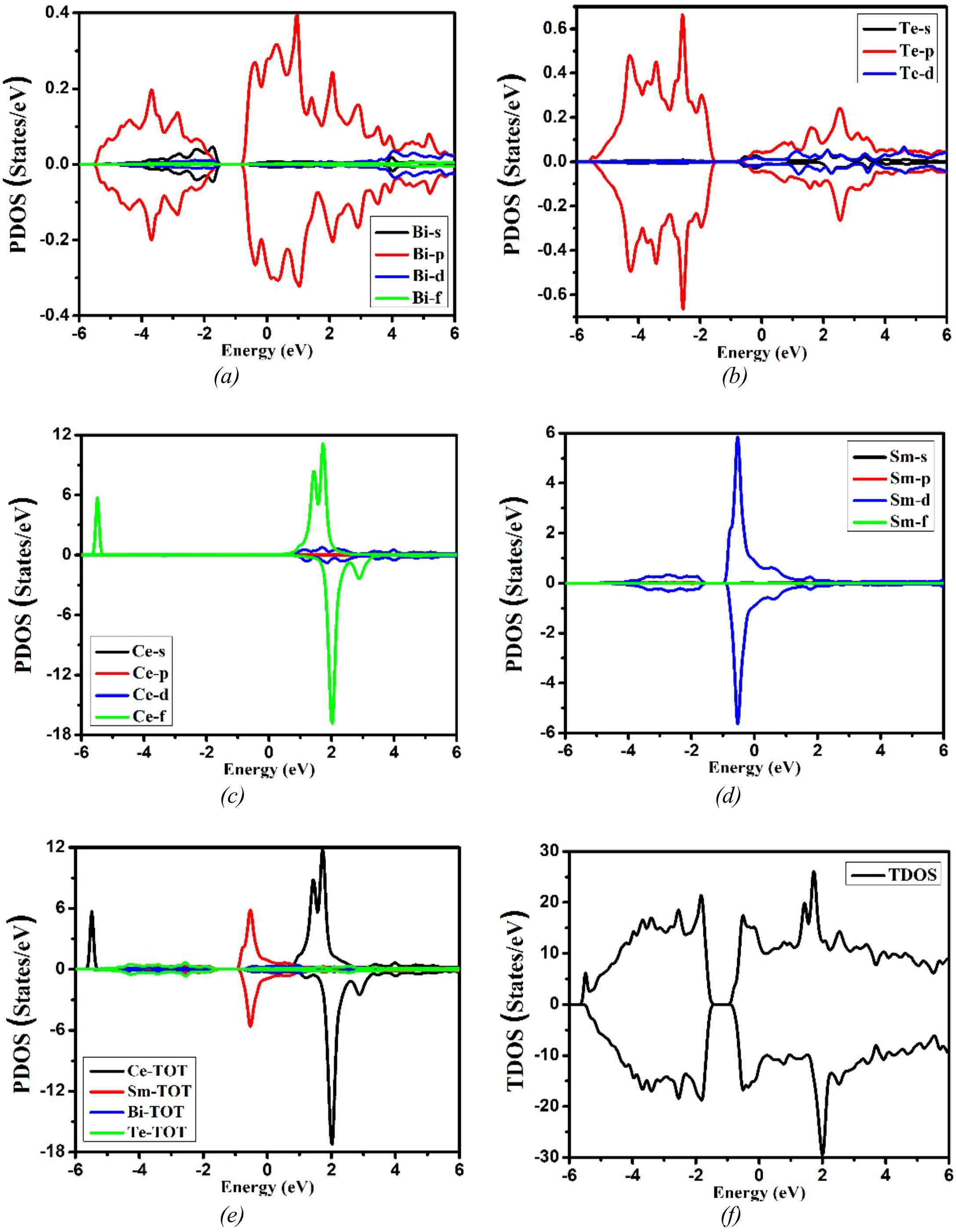

(a) *(b)*

(c) *(d)*

(e) *(f)*

Fig. 2. Total and partial density of states Bismuth Telluride (Bi_2Te_3).

3.2. Optical properties

3.2.1. Dielectric function dispersion

The complex dielectric function and the energy band structure, both parameters depend on each other. The electronic wave functions and energy eigenvalues are needed to calculate the frequency-dependent dielectric function (dispersion). Each inter-band and intra-band transitions are thought about to be a very important feature for finding the optical response of the material. The intra-band transitions are thought about to be necessary just for the case of metals, however, the inter-band transitions (either direct or indirect) are terribly sensitive towards electromagnetic interaction.

The optical reaction in the presence of an outside electric field of any actual framework can be indicated regarding dielectric work with $\varepsilon(\omega) = \varepsilon_1 (\omega) + i\varepsilon_2 (\omega)$ numerical articulation. The Kramer–Kronig connection has been executed to ascertain the genuine piece of dielectric work $\varepsilon_1 (\omega)$ that clarify the scattering of light from issue surface. The ingestion of electromagnetic radiations has been clarified by the mind-boggling dielectric capacity of the nonexistent part $\varepsilon_2 (\omega)$. The dielectric constants of recurrence subordinate with genuine and fanciful parts are going with one another by Kramer–Kronig connection as figured underneath.

$$\varepsilon_1(\omega) = 1 + \frac{2}{\pi}\, P\int_0^{\infty} \frac{\omega'\varepsilon_2\omega'}{\omega'^2-\omega^2}\, d\omega' \tag{i}$$

$$\varepsilon_2(\omega) = \frac{e^2 h'}{\pi m^2 \omega^2} \sum_{v,c} \int_{BZ}^{\infty} |M_{cv}(k)|^2\, \delta[\omega_{cv}(k) - \omega] d^3k \tag{ii}$$

where the fundamental necessary value is denoted by P and k is the wave vector that is hard inside the main Brillion zone (BZ) limit. The Kramer–Kronig relation is used to constituent of dielectric tensor among genuine and nonexistent parts to clarify the photon relationship**.** Optical responses and spectra have been investigated in the present study at equilibrium lattice constant for the energy range from 0-14.0 eV. Fig. 3(a) shows the real part of dielectric function $\varepsilon_1(\omega)$ in three different independent -x,-y and -z directions as function of photon energy. Real part of dielectric function calculated for three different crystallographic axes of Bi_2Te_3 shows large anisotropy in the energy range 0-0.80ev. Beyond this range $\varepsilon_1(\omega)$ increases till energy 2 eV. After energy 2 eV anisotropy becomes almost becomes negligible with very small value of $\varepsilon_1(\omega)$ for different directions. The anisotropy is maximum at around 0.40 eV for x- and y- and at around 0.75 eV for z-. These peaks correspond to energy transition between some orbitals corresponding to certain energy because $\varepsilon_1(\omega)$ is related to density of states.

Fig 3(b) shows the variation of imaginary part along x-, y- and z- directions with variation of photon energy in eV. The x- and y- component of $\varepsilon_2(\omega)$ represented by black and red line show almost similar behavior with the change in energy. When energy starts to increase from 0ev x- and y- component of $\varepsilon_2(\omega)$ show a peak at almost 0.2 eV. After that with the further increase in photon energy$\varepsilon_2(\omega)$ for x- and y- components becomes almost 0 at photon energy almost close to 1.7 eV and then again it increases from energy range 1.7-3.4ev. After this $\varepsilon_2(\omega)$ for x- and y- component almost becomes constant till 6.3ev. The imaginary part of dielectric function $\varepsilon_2(\omega)$ increases from 6.3-7.3ev energy range. Beyond this range $\varepsilon_2(\omega)$ for x- and y- components becomes constant. The z-component of $\varepsilon_2(\omega)$ represented by blue line shows a little different behavior as compared to the x- and y- component. The y-component increase rapidly and reaches its maximum value at photon energy 0.2ev and from here its starts to decrease rapidly. At photon energy 1.6ev it once again starts to increase a bit till photon energy 3.5ev. Beyond this energy it again becomes constant beside one peak which is shown at photon energy 6.3-7.7ev. Beyond this range z-component becomes constant. These Peaks are due to inter band transitions from valence band to conduction band.

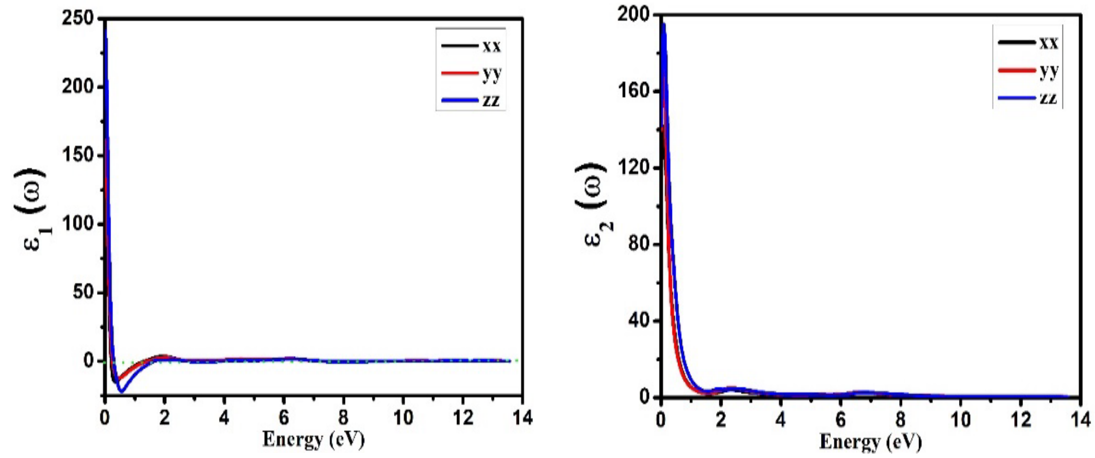

(a) *(b)*

Fig. 2. Real and imaginary parts of Bismuth Telluride (Bi_2Te_3).

3.2.2. Refractive index n(ω) and extinction coefficient k(ω)

The other optical boundaries like refractive file n (ω) and annihilation coefficient k(ω) are identified with the photon energy-matter collaboration and determined as far as $\varepsilon_1(\omega)$ and $\varepsilon_2(\omega)$ as given underneath.

$$n(\omega) = \left[\frac{\varepsilon_1(\omega)}{2} + \frac{\sqrt{\varepsilon_1{}^2(\omega)+\varepsilon_2{}^2(\omega)}}{2}\right]^{1/2} \quad \text{(iii)}$$

$$k(\omega) = \left[\frac{-\varepsilon_1(\omega)}{2} + \frac{\sqrt{\varepsilon_1{}^2(\omega)+\varepsilon_2{}^2(\omega)}}{2}\right]^{1/2} \quad \text{(iv)}$$

The complex refraction coefficient is the copy of complex dielectric consistent and communicated as

$$\bar{n}(\omega) = n(\omega) + ik(\omega) \quad \text{(v)}$$

The genuine part (real part) speaks to the refractive record n (ω) and the nonexistent piece (imaginary part) of refraction is extinction coefficient k (ω).

Figure 4(a) shows that refractive index (n) almost shows quite similar behavior in all crystallographic directions x-, y- and z-axis. It keeps on decreasing with the increase in photon energy. It is observed that refractive index (n) decreases abruptly in all three directions till photon energy 1.2ev,1.3ev and 1.4ev for x-z- and y-directions, respectively. Beyond this energy refractive index (n) displays fluctuations till photon energy 14ev.

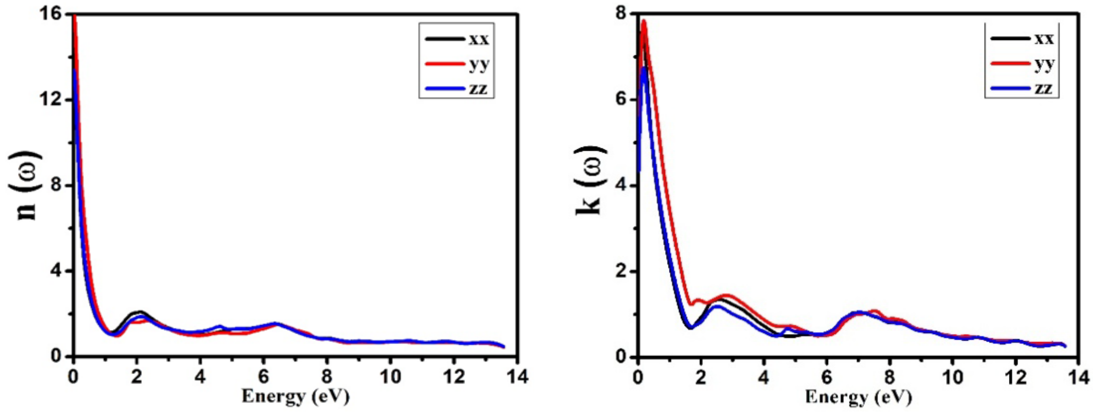

(a) *(b)*

Fig. 3. Refractive index and extinction coefficent of Bismuth Telluride (Bi_2Te_3).

The extinction coefficient k (ω) has a similar behavior as $\varepsilon_2(\omega)$, imaginary part of dielectric function. From figure 3 (b) it is quite evident that k(ω) decreases continuously with increase in energy in all three directions since the first peak which is observed at almost 0.25ev approximately. The highest value of k (ω) at that energy is along y-axis which is represented by the red line in the figure. At energy 1.8ev k(ω) along x- and z- direction starts to increase till 2.5ev and then decreases continuously. While along y-axis k(ω) starts to increase from 2.2ev up to almost 3.oev and then decreases continuously. At energy close to 6.0ev, the values of k(ω) along all the directions increases till energy 7.1ev. Beyond this energy k(ω) goes on decreasing continuously till the end. The variations in the values of $\varepsilon_2(\omega)$ and k(ω) might be due to theoretical approximations.

3.2.3. Absorption coefficient α(ω) and optical conductivity σ(ω)

The absorption coefficient decides how far into a material light of a specific frequency can infiltrate before it is retained. In a material with a low ingestion coefficient, light is just ineffectively assimilated, and if the material is sufficiently slim, it will seem straightforward to that frequency. The retention coefficient relies upon the material and furthermore on the frequency of light which is being consumed. Semiconductor materials have a sharp edge in their retention coefficient, since light which has energy underneath the band hole does not have adequate energy to energize an electron into the conduction band from the valence band. Thusly, this light is not assimilated.

The absorption coefficient α(ω) is another factor that calculates where the material is suitable for optoelectronic applications. It measures the decay of photon energy per centimeter into the material. The behavior of absorption coefficient α (ω), the imaginary part of the dielectric constant ε_2 (ω) and extinction coefficient k (ω) are consistent that shows the Kramer-Kronig relation and tensor matrix are equally solve the optical parameters. Moreover, the absorption is linked with extinction coefficient through relation.

$$\alpha(\omega) = 4\pi k(\omega)/\lambda$$

This relation shows the absorption coefficient is wave vector time the extinction coefficient. From fig 4, It is very much clear that absorption along x- and z-direction is almost similar but along y-direction it shows a little different behavior. Absorption coefficient increases rapidly with a little increase in photon energy. The first peak is seen at almost photon energy 0.6ev,0.7ev along x- and z-direction, respectively. In the energy range 2.2-5.3ev the absorption along x- and z-direction shows a little different behavior from each other. In this range absorption along x-direction is more than along z-direction. But beyond this range the absorption again becomes very much similar along x- and z- direction. The absorption coefficients exhibit smaller fluctuations around 6ev along x- and z- directions. The maximum value of absorption along x- and z-direction is seen at photon energy 7ev.

It can also be seen from the fig 2.5 that red line which is representing absorption along y-direction increases rapidly at the start when photon energy increases. The first peak is observed at photon energy 0.8ev along y-direction. With the further increase in energy absorption exhibits smaller fluctuations around 6.2ev and becomes maximum at 7.2ev. It is also apparent that absorption is relativity higher along y-direction which might be due to indirect band gap. It was observed from the absorption spectra that the absorption lies in visible and near UV region of the radiation which makes this material interesting and could be utilized for its application in optoelectronics.

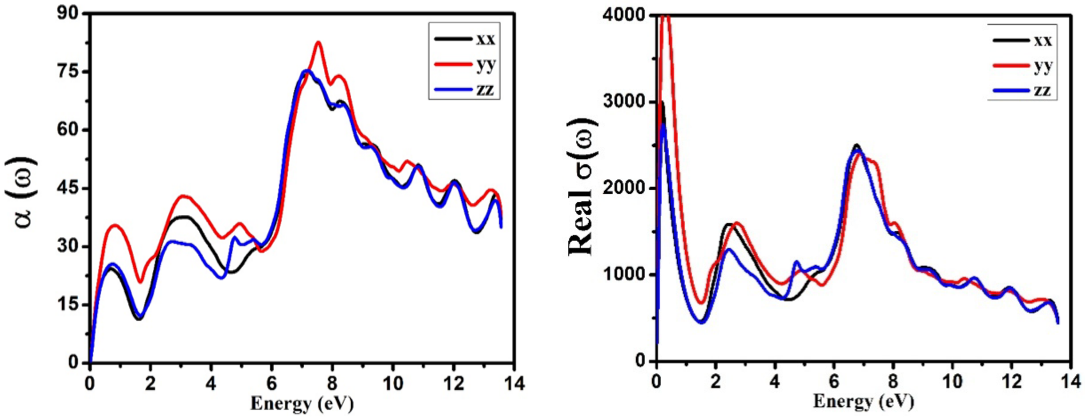

(a) *(b)*

Fig. 4. Absorption coefficent and real optical conductivity of Bismuth Telluride (Bi_2Te_3).

Optical conductivity is the proportion of the measure of opticalflow a material can convey or its capacity to convey a flow. Opticalconductivity is otherwise called explicit conductance. Conductivity is an inherent property of a material.Opticalconductivity is indicated by the σ and has SI units of siemens per meter (S/m). In opticaldesigning, the Greek letter κ is utilized. At times the Greek letter γ speaks to conductivity. In water, conductivity is regularly announced as explicit conductance, which is a measure contrasted with that of unadulterated water at 25°C.

The optical conductivity σ (ω) is the flow of carriers when surplus photon energy delivered to the electrons in the valences. The electrons move to the conduction band by overcoming the influence of nuclei and increase the optical current or photocurrent. During light-matter interaction, the absorption, transmission, and conduction take place simultaneously. When the energy of the incident exceeds from band gap, the electrons kinetic energy increases and that also increase the electrical conductivity. Moreover, the optical conductivity is related to the dielectric constant by relation $\varepsilon(\omega) = \varepsilon_0 + i\,\sigma(\omega)/\omega$, here ε_0 and ω are the permittivity of the free space and plasma frequency. Therefore, the optical conductivity related to the imaginary part of dielectric constant.

Figure 4(b) shows how optical conductivity (σ) varies with the increase in photon energy. It can be seen in the graph that optical conductivity along all the crystallographic directions show similar trend. The optical conductivity shows first peak with almost negligible increase in photon energy. The first peak along x- and z- direction is seen at energy 0.1ev while along y-axis is seen at 0.2ev. After this optical conductivity σ decreases almost up to 1.7ev photon energy. The second highest peak along all the directions is observed at energy almost equal to 7.0ev along x- and z- direction while along y-axis peak is seen at energy 7.1 ev. Beyond this energy the optical conductivity σ keeps on decreasing till photon energy 14ev.

3.2.4. Reflectivity R(ω)

Reflectivity is an optical property of material, which portrays how much light is reflected from the material according to a measure of light occurrence on the material. The reflection happens consistently on the outside of the material, for the light-diffusing (clear) materials additionally in the volume of the material.

Reflectivity relies upon the frequency of light, bearing of the occurrence and mirrored light, polarization of light, sort of the material (metal, plastic, and so forth), substance synthesis structure of the material, and condition of the material and its surface (temperature, surface harshness, level of oxidation and defilement). It can be calculated from refractive index and extinction coefficient by using the following relation.

$$R = \frac{n-1^2+k^2}{n+1^2+k^2} \tag{vi}$$

Figure 5 shows the variation of reflection spectra along three different crystallographic axes with photon energy. If we look at the figure 2.3, reflectivity along x- and z- component shows almost similar behavior while y-component shows a little different behavior. The value of reflectivity R(ω) along x- and y- directions decreases rapidly from its maximum value to 0.1 at photon energy 1.6ev and 1.65ev for x- and z-component, respectively. After this reflectivity shows fluctuations till energy 14ev for x- and z- components. These fluctuations might be due to inter-band transitions. The y- component of reflectivity coefficient which is represented by red line shows a shoulder at photon energy 0.25ev and then decreases rapidly to value 2.2 and then shows a shoulder at photon energy 1.75ev. After this it increases with variations from 1.8ev to almost 14ev. At 14ev reflectivity value along y-direction is greater as compared to x- and z-direction.

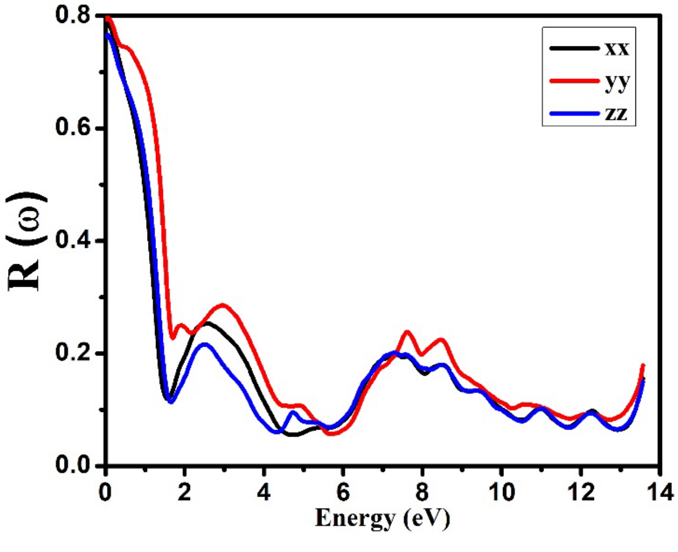

Fig. 5. Reflectivity of Bismuth Telluride (Bi_2Te_3).

3.2.5. Energy loss function L (ω)

Energy loss function L(ω) represents the energy loss when free charges move fast and travel through the material. The variation in L(ω) with photon energy has been shown in figure 6.

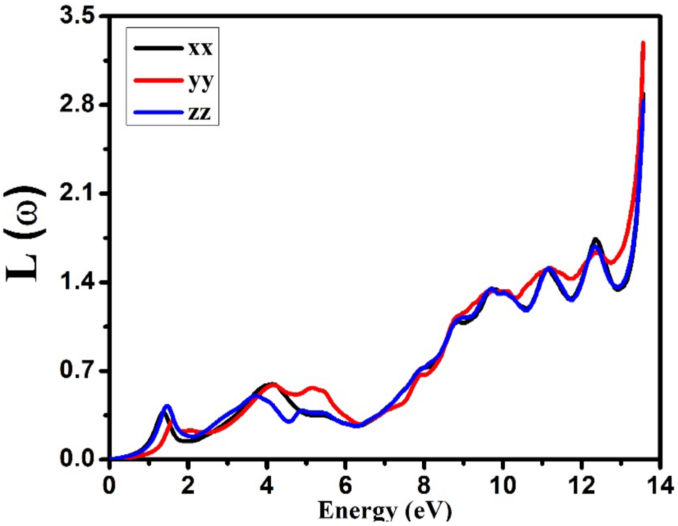

Fig. 6. Energy loss function of Bismuth Telluride (Bi_2Te_3).

The peaks in energy loss spectra L (ω) gives the information about plasma frequency (ω_{pl}) for the material. Plasma frequencies describe the nature of material, as above this frequency material behaves like a dielectric [$\varepsilon_1(\omega) > 0$] and below this frequency, it behaves as metallic [$\varepsilon_1(\omega) < 0$]. It means the energy loss spectra, L (ω) describe the point of transition from dielectric property to metallic property of the material. Energy loss spectra clearly show the maximum peaks around 13.2ev along x-y- and z- directions for the compound which indicates a larger loss along y-direction as compared to x- and z-directions.

3.3. Thermoelectric properties

The search for suitable thermoelectric materials has necessitated the requirement of demonstrating exciting properties. They should, for example, have extremely low thermal conductivities while having high electrical conductivities and Seebeck coefficients. As previously reported [27,28], the studied materials contain heavy elements and have low lattice thermal conductivities. Because all of these coefficients are correlated, scientists will find it difficult to optimise their qualities. The function of the electronic band structure in determining thermal and electronic transport characteristics has been established, and it has been discovered that solids with partially filled Fermi energy levels (metals) produce less efficient thermoelectric devices.

Those with a gap between conduction and valence states (exhibiting semiconducting nature) are more capable when it comes to thermoelectric conversions. Because the bandgap affects the transport characteristics, we used the GGA+U potential to precisely compute the bandgap. Figure 1 shows the estimated transport characteristics versus temperature (K). Figure 5 6. The available free carriers in the conduction band are measured by electrical conductivity $\left(\sigma / t\right)$. For practical applications of thermoelectric devices, high electrical conductivity controls the Joule heating effect [29-31].

Figure 7 shows the calculated electrical conductivity. 5 (a, b) (a, b). The chemical potential signifies the energy needed to accept electrons by facing the repulsion of already existing electrons in the valence shell. Its positive and negative values distinguish p-type from -type behaviour. There is a linear increase in the σ/τ up to 850 K as at high-temperature as bond breaks and more carriers are available for conduction.

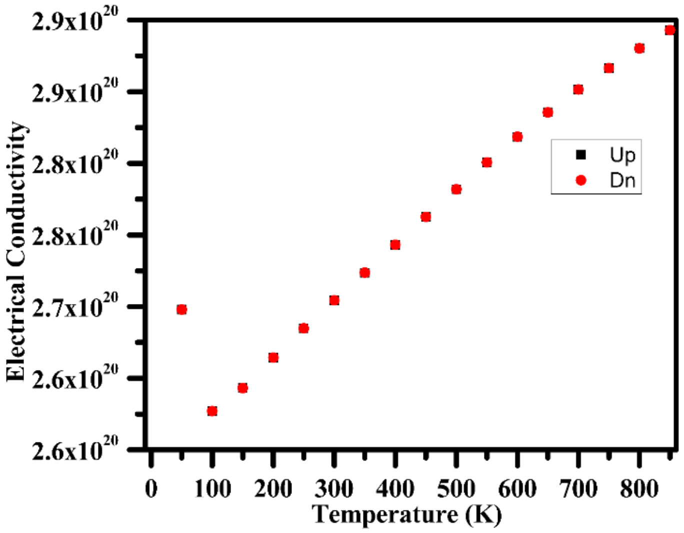

Fig. 7. (a, b) Electrical conductivity versus temperature.

Heat transferred in semiconductors in two modes; electronic as well as phonons that causes due to lattice vibration. Thus, the thermal conductivity ($\kappa = \kappa l + \kappa e$) is the mutual measure of electrons and lattice vibrations [32]. Fig. 8 shows the behavior of thermal conductivity (κ/τ), which is similar to σ/τ but its value is 10^{-4} times less than σ/τ. The Wiedemann-Franz law $LT=k/\sigma$ [33] explains it using thermal to electrical conductivity (10^{-4}). Therefore, low thermal conductivity makes them suitable for transport properties.

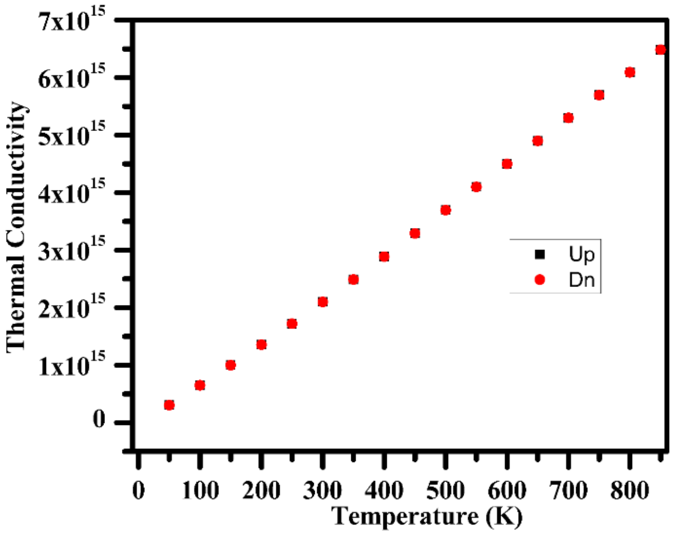

Fig. 8. Thermal conductivity plotted versus temperature.

The high values of the Seebeck coefficient (S) confirm the material's suitability for thermoelectric device application. From Fig. 9, the n-type nature of studied material is categorized by negative values of S. The S decreases almost linearly up to 850 K. The value of S is greater for both up and down is the same. The Seebeck coefficient is the potential gradient concerning a temperature between two dissimilar contacts of metals. The increasing temperature decreases the number of collisions of electrons or the thermalization effect. This thermalization effect, Coulomb repulsion among electrons develops potential gradient which decreases the Seebeck coefficient.

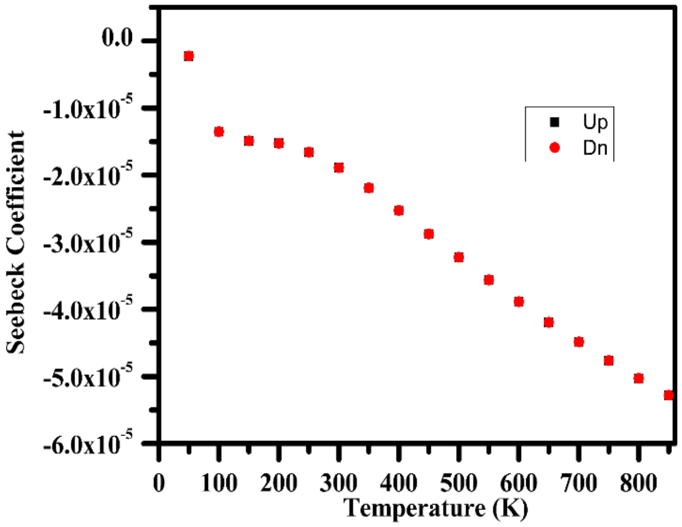

Fig. 9. Seebeck coefficient verses temperature.

The power factor (S2σ/τ) illustrate the performance of the thermoelectric device in terms of σ/τ and S as illustrated in Fig. 10. The PF of Sm/Ce co doped Bi2Te3 has a slightly higher value than the up, and its value increases with increasing temperature for both spin. This is the metallic material and favorably used for solar cells and other optoelectronics like surgical equipment due to maximum absorption in the ultraviolet region of the spectrum. For thermoelectric, this material may be used for thermoelectric generators.

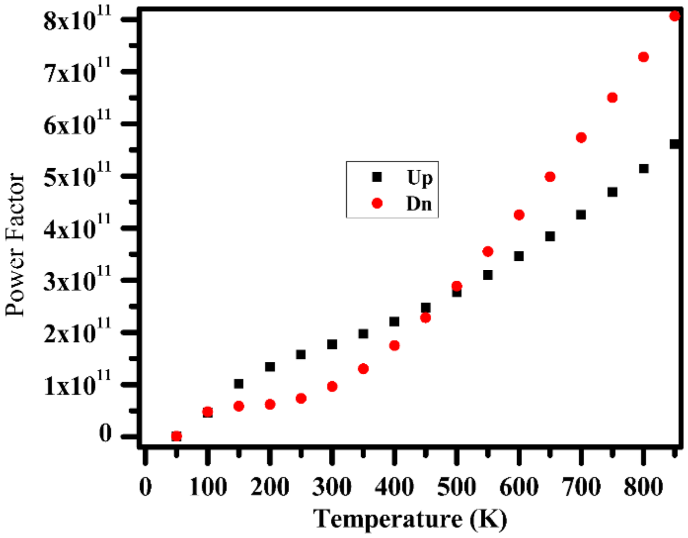

Fig. 10. Power factor plotted versus temperature.

4. Conclusion

In conclusion, we have analytically discussed the optoelectronic and thermoelectric properties of SM/Ce co-doped Bi2Te3. The material shows the metallic nature. The absorption and polarization of light take place in the infra-red and ultraviolet region, which increases its importance for optoelectronic applications.

Moreover, the reflection and optical loss of light are small in the UV region. The thermal conductivity to electrical conductivity ratio is minimal (10^{-5}), showing their importance for transport properties.

Acknowledgment

The authors H. Elhosiny Ali extend their appreciation to the Research Center for Advanced Materials Science (RCAMS), King Khalid University, Saudi Arabia, for funding this work under grant number RCAMS/KKU/012-22.

References

[1] H.J. Goldsmith Theory of thermoelectric devices Applications of thermoelectricity, Methuen & Co Ltd, London (1960)

[2] D.M. Rowe General principles and basic considerationD.M. Rowe (Ed.), Thermoelectrics handbook: macro to nano, Taylor & Francis, Boca Raton, FL (2006); https://doi.org/10.1201/9781420038903.sec1

[3] H.J. Goldsmith Conversion efficiency and figure-of-merit D.M. Rowe (Ed.), CRC handbook of thermoelectrics: macro to Nano, CRC Press, Boca Raton, FL (1995); https://doi.org/10.1201/9781420049718.ch3

[4] S.I. Kim, et al. Dense dislocation arrays embedded in grain boundaries for high-performance bulk thermoelectrics Science, 348 (2015), p. 109; https://doi.org/10.1126/science.aaa4166

[5] N. Madar, et al. High thermoelectric potential of Bi2Te3 alloyed GeTe- rich phases J Appl Phys, 120 (2016), Article 035102; https://doi.org/10.1063/1.4958973

[6] Y. Sadia, et al. Criteria for extending the operation periods of thermoelectric converters based on IV-VI compounds J Solid State Chem, 241 (2016), pp. 79-85; https://doi.org/10.1016/j.jssc.2016.06.006

[7] D. Ben-Ayoun, et al. High temperature thermoelectric properties evolution of Pb1-xSnxTe based alloys J Alloys Compd, 722 (2017), pp. 33-38; https://doi.org/10.1016/j.jallcom.2017.06.075

[8] O. Meroz, et al. Development of Bi2Te2.4Se0.6 alloy for thermoelectric power generation applications J Alloys Compd, 679 (2016), pp. 196-201; https://doi.org/10.1016/j.jallcom.2016.04.072

[9] Y. Sadia, et al. Thermoelectric properties in the quasi-binary MnSi1.73-FeSi2 system J Electron Mater, 44 (2015), p. 1637; https://doi.org/10.1007/s11664-014-3500-z

[10]. MTI Corp - Leading provider of lab equipments and advanced crystal substrates. MTI Corp - Leading provider of lab equipments and advanced crystal substrates. (2020). Retrieved 29 December 2020, from https://www.mtixtl.com/bi2te3singlecrystal.aspx.

[11]. Meija, J., Coplen, T., Berglund, M., Brand, W., De Bièvre, P., & Gröning, M. et al. (2016). Atomic weights of the elements 2013 (IUPAC Technical Report). Pure and Applied Chemistry, 88(3), 265-291. https://doi.org/10.1515/pac-2015-0305; https://doi.org/10.1515/pac-2015-0305

[12] B. Poudel, et al. High-thermoelectric performance of nanostructured bismuth antimony telluride bulk alloys Science, 320 (2008), p. 634; https://doi.org/10.1126/science.1156446

[13] Y. Ma, et al. Enhanced thermoelectric figure-of-merit in p-type nanostructured bismuth antimony tellurium alloys made from elemental chunks Nano Lett, 8 (2008), p. 2581; https://doi.org/10.1021/nl8009928

[14] W.-S. Liu, et al. Thermoelectric property studies on Cu-doped n-type CuxBi2Te2.7Se0.3 nanocomposites Adv. Energy Mater., 1 (2011), p. 577; https://doi.org/10.1002/aenm.201100149

[15] J. Horak, J. Navartils, Z. Stary Lattice point defects and free-carrier concentration in Bi2+xTe3 and Bi2+xSe3 crystals J Phys Chem Solid, 53 (1992), p. 1067; https://doi.org/10.1016/0022-3697(92)90079-S

[16] D.O. Scanlon, et al. Controlling bulk conductivity in topological insulators: key role of anti-site defects Adv Mater, 24 (2012), p. 2154; https://doi.org/10.1002/adma.201200187

[17] Tan, et al. Synergistically optimized thermoelectric performance in Bi0.48Sb1.52Te3 by hot deformation and Cu doping ACS Appl Energy Mater, 2 (2019), pp. 6714-6719; https://doi.org/10.1021/acsaem.9b01207

[18] Kim, et al. Stress-induced change of Cu-doped Bi2Te3 thin films for flexible thermoelectric applications Mater Lett, 270 (2020), p. 127697; https://doi.org/10.1016/j.matlet.2020.127697

[19] Padmanathan, et al. Amorphous framework in electrodeposited CuBiTe thermoelectric thin films with high room-temperature performance ACS Appl. Electron. Mater., 3 (2021), pp. 1794-1803; https://doi.org/10.1021/acsaelm.1c00063

[20] H.J. Goldsmid Recent studies of bismuth telluride and its alloys J Appl Phys, 32 (1961), p. 2198; https://doi.org/10.1063/1.1777042

[21] P. Hohenberg, W. Kohn Inhomogeneous electron gas Phys. Rev., 136 (1964), pp. B864-B871; https://doi.org/10.1103/PhysRev.136.B864

[22] W. Kohn, L.J. Sham Self-consistent equations including exchange and correlation effects Phys. Rev., 140 (1965), pp. A1133-A1138; https://doi.org/10.1103/PhysRev.140.A1133

[23] P. Blaha, K. Schwarz, G.K.H. Madsen, D. Kvasnicka, J. Luitz, R. Laskowski, F. Tran, L.D. Marks

WIEN2k, An Augmented Plane Wave þ Local Orbitals Program for Calculating Crystal Properties Karlheinz Schwarz, Techn Universit€at Wien, Austria (2018) ISBN 3-9501031-1-2

[24] P. Blaha, K. Schwarz, P. Sorantin, S. Trickey Full-potential, linearized augmented plane wave programs for crystalline systems Comput. Phys. Commun., 59 (1990), pp. 399-415; https://doi.org/10.1016/0010-4655(90)90187-6

[25] A. Jain, S.P. Ong, G. Hautier, W. Chen, W.D. Richards, S. Dacek, S. Cholia, D. Gunter, D. Skinner, G. Ceder Commentary: the materials project: a materials genome approach to accelerating materials innovation APL Mater., 1 (2013); https://doi.org/10.1063/1.4812323

[26] J.P. Perdew, K. Burke, M. Ernzerhof Generalized gradient approximation made simple Phys. Rev. Lett., 77 (1996), pp. 3865-3868; https://doi.org/10.1103/PhysRevLett.77.3865

[26] M. Sajjad, N. Singh, J.A. Larsson AIP Adv., 10 (2020); https://doi.org/10.1063/1.5133711

[27] D. Singh, M. Sajjad, J.A. Larsson, R. Ahuja Results Phys., 19 (2020); https://doi.org/10.1016/j.rinp.2020.103584

[28] M. Hassan, A. Shahid, Q. Mahmood Structural, electronic, optical and thermoelectric investigations of antiperovskites A3SnO (A = Ca, Sr, Ba) using density functional theory Solid State Commun., 270 (2018), pp. 92-98; https://doi.org/10.1016/j.ssc.2017.11.019

[29] M. Rizwan, A. Ali, Z. Usman, N.R. Khalid, H.B. Jin, C.B. Cao Structural, electronic and optical properties of copper-doped SrTiO3 perovskite: a DFT study Phys. B Condens. Matter, 552 (2019), pp. 52-57; https://doi.org/10.1016/j.physb.2018.09.022

[30] H.A.R. Aliabad, M. Ghazanfari, I. Ahmad, M.A. Saeed Ab initio calculations of structural, optical and thermoelectric properties for CoSb3 and ACo4Sb12 (A= La, Tl and Y) compounds Comput. Mater. Sci., 65 (2012), pp. 509-519; https://doi.org/10.1016/j.commatsci.2012.08.013

[31] Q. Mahmood, M. Hassan, S.H.A. Ahmed, A. Shahid, A. Laref Study of optoelectronic and thermoelectric properties of BaSiO3 perovskite under moderate pressure for energy renewable devices applications J. Phys. Chem. Solid., 20 (2018), pp. 87-95; https://doi.org/10.1016/j.jpcs.2018.04.024

[32] M.E. Fine, N. Hsieh Wiedermann-franz-lorenz relation in highly electronic-conducting oxides J. Am. Ceram. Soc., 57 (1974), pp. 502-503; https://doi.org/10.1111/j.1151-2916.1974.tb11407.x